

Conversion Layer Controls the Evolution of Magnetic Deflections Near the Alfvén Surface

DOMINIC PAYNE,¹ MOJTABA AKHAVAN-TAFTI,¹ JOSHUA GOODWILL,² SAMUEL BADMAN,³ RIDDHI BANDYOPADHYAY,² SUBASH ADHIKARI,² WILLIAM MATTHAEUS,² GARY ZANK,⁴ CHEN SHI,⁵ MICHAEL STEVENS,³ ROBERTO LIVI,⁶ YEIMY RIVERA,³ AND KRISTOFF PAULSON³

¹*Climate and Space Sciences and Engineering, University of Michigan, Ann Arbor, MI, 48109*

²*Department of Physics and Astronomy, University of Delaware, Newark, DE, 19716*

³*Center for Astrophysics, Harvard & Smithsonian, Cambridge, MA, 02138*

⁴*University of Alabama Huntsville, Huntsville, AL, 35899*

⁵*Department of Physics, Auburn University, Auburn, AL, 36849*

⁶*University of California Berkeley Space Sciences Laboratory, Berkeley, CA, 94720*

ABSTRACT

We examine the statistics of Alfvénic deflections in both sub-Alfvénic and super-Alfvénic solar wind with particular focus on a common parameter that underlies the definition of switchbacks: the magnetic deflection angle θ_{def} . Our findings are in general agreement with earlier studies that suggest magnetic deflection angles of $\theta_{def} > 90$ degrees are very unlikely to occur in sub-Alfvénic regimes. We find that the upper limit of θ_{def} exhibits an identifiable trend with the Alfvén Mach number M_a , suggesting that gradual steepening of Alfvénic deflections with increasing M_a is a plausible mechanism controlling deflection angles in the young solar wind. Further analysis reveals that large velocity fluctuations ($\delta v/v > 1$) tend to be important in the largest sub-Alfvénic magnetic deflections with increasing contributions from δv_{\parallel} very close to $M_a = 1$, while virtually no magnetic deflections in the super-Alfvénic regime exhibit such large velocity perturbations. We also determine the local ratio of radial Poynting flux S_R to kinetic energy flux K_R and find that large sub-Alfvénic deflection angles tend to be dominated by S_R , while super-Alfvénic deflections are eventually dominated by the K_R associated with the radial solar wind flow. Our results show that within the vicinity of the Alfvén surface (where $M_a = 1$), there is a critical region of parameter space within which $\delta v \sim v_a$ and $K_R/S_R \sim 1$. We refer to this region (where $|\log_{10}(M_a)| < 0.2$) as the conversion layer. The conversion layer may play a significant role in the evolution of magnetic deflections by providing the medium for converting magnetic energy to particle energy and likely driving the formation of magnetic switchbacks in super-Alfvénic solar wind.

1. INTRODUCTION

Ever since the Parker Solar Probe (PSP) observed localized Alfvénic structures with correlated radial velocity spikes and magnetic field reversals in the young solar wind (Bale et al. 2019; Kasper et al. 2019), the origin location and generation mechanism of these so-called “switchbacks” have been topics of interest to the heliophysics community. One potentially relevant threshold responsible for switchback generation is the Alfvén critical surface R_a (Chhiber et al. 2024), where the ratio of local solar wind bulk velocity to the local Alfvén speed (also known as the Alfvénic mach number M_a) is equal to one. Results from recent encounters of the sub-Alfvénic solar wind ($M_a < 1$) suggest that switchbacks cease to exist below R_a (Bandyopadhyay et al. 2022; Akhavan-Tafti & Soni 2024), and therefore switchbacks may be the result of an in-situ generation mechanism that manifests at or beyond the $M_a = 1$ threshold (Akhavan-Tafti & Soni 2024).

It is not yet clear whether full switchbacks form at the Alfvén surface or whether they form gradually from other types of Alfvénic deflections that do not meet more constrained definitions of switchbacks until they have propagated beyond R_a . If magnetic deflections exceeding a 90 degree deflection angle can form gradually from initially sub-Alfvénic

magnetic deflections below the 90 degree threshold, then the switchback generation mechanism could occur well below R_a , forming a seed structure that ultimately steepens into a mature switchback beyond R_a .

In the following study, we use a variety of intervals from encounters 13-23 to examine the characteristics of magnetic deflections, particularly as a function of M_a to explore what role the $M_a = 1$ threshold plays in switchback formation in the solar wind. This study is complementary to and was conducted in collaboration with [Goodwill et al. \(2025\)](#), who examined the statistical dependence between M_a , the switchback parameter (related to the magnetic deflection angle) and deflections in radial velocity and magnetic field. Although this study and that of [Goodwill et al. \(2025\)](#) differ in the range of PSP encounters used and the specific methods for identifying deflections, both studies approach similar conclusions regarding the overall trends with respect to M_a . Section 2 describes the instruments used for data collection, definitions of key parameters, and the criteria used to select and filter deflection data. In section 4, we present our initial findings of the distribution of magnetic deflection angles as a function of M_a and radial distance from the sun. Section 5 examines the velocity deflections associated with the distribution of magnetic deflections as well as the ratio of radial energy flux densities, and how these parameters differ in sub- vs super-Alfvénic regimes and with magnetic deflection angle. In section 6, we discuss the implications of our results for switchback formation and finally summarize our findings in section 7.

2. DATA AND METHODS

The magnetic field data in this study come from the FIELDS ([Bale et al. 2016](#)) instrument suite on PSP, which provides vector magnetic field measurements up to a 290 sample per second cadence. The ion velocity data comes from the SWEAP instrument suite on PSP ([Kasper et al. 2016](#)), specifically the Solar Probe Analyzer for ions ([Livi et al. 2022](#)). The density is determined via the quasi-thermal noise (QTN), which comes from the Radio Frequency Spectrometer (RFS) included with FIELDS ([Pulupa et al. 2017](#)). All data products used in this study are interpolated to match the time cadence of SPAN-I velocity data before any variables or time-averages are computed.

Our objective is to explore how Alfvénic deflections systematically differ for a range of M_a values that span the $M_a = 1$ threshold. M_a is calculated based on the mean proton velocity magnitude $\langle |v_p| \rangle$ and the Alfvén speed $v_a = \frac{\langle |B| \rangle}{\sqrt{\mu_0 m_i n}}$ where $\langle |B| \rangle$ is the mean magnetic field magnitude, μ_0 is the vacuum magnetic permeability, m_i is the proton mass, n is the density derived from QTN, and angled brackets indicate a 10 minute average.

$$M_a = \frac{\langle |v_p| \rangle}{v_a}$$

From a variety of PSP perihelia we select intervals that are either sub-Alfvénic ($M_a < 1$) or super-Alfvénic ($M_a > 1$) for at least 6 consecutive hours and we include an additional collection of “near-Alfvénic” intervals where M_a is close to unity to get sufficient data close to the Alfvén surface (see supplemental material).

Some studies tend to have more strict definitions of switchbacks ([Akhavan-Tafti et al. 2021](#)), while others tend to only consider the deflection angle as the defining feature ([de Wit et al. 2020](#)). We do not exclude deflection angles below 90 degrees from our selections. However, we do filter out any uncorrelated magnetic and velocity fluctuations with the condition that both $\delta v/v > 0.05$ and $\delta B/B > 0.05$. The $\delta B/B$ term is a scalar quantity defined explicitly below.

$$\frac{\delta B}{B} = \frac{|\vec{B} - \langle \vec{B} \rangle|}{|\langle \vec{B} \rangle|}$$

where \vec{B} is the vector magnetic field (interpolated to the SPAN-I velocity data cadence) and $\langle \vec{B} \rangle$ is the mean vector magnetic field using a 10 minute averaging window. $\delta v/v$ is defined in the same way, using the vectors \vec{v} and $\langle \vec{v} \rangle$. The magnetic deflection angle θ_{def} is the angle between the vector magnetic field measurement and the mean vector magnetic field over the 10 minute averaging window, defined below.

$$\theta_{def} = \arccos \left(\frac{\vec{B} \cdot \langle \vec{B} \rangle}{|\vec{B}| |\langle \vec{B} \rangle|} \right)$$

The following work also examines the statistics of the energy flux densities associated with the distribution of magnetic deflections with varied M_a . The two most relevant to the the solar wind are the Poynting flux \vec{S} associated with the transport of electromagnetic energy and the ion kinetic energy flux \vec{K} associated with the bulk flow of ion

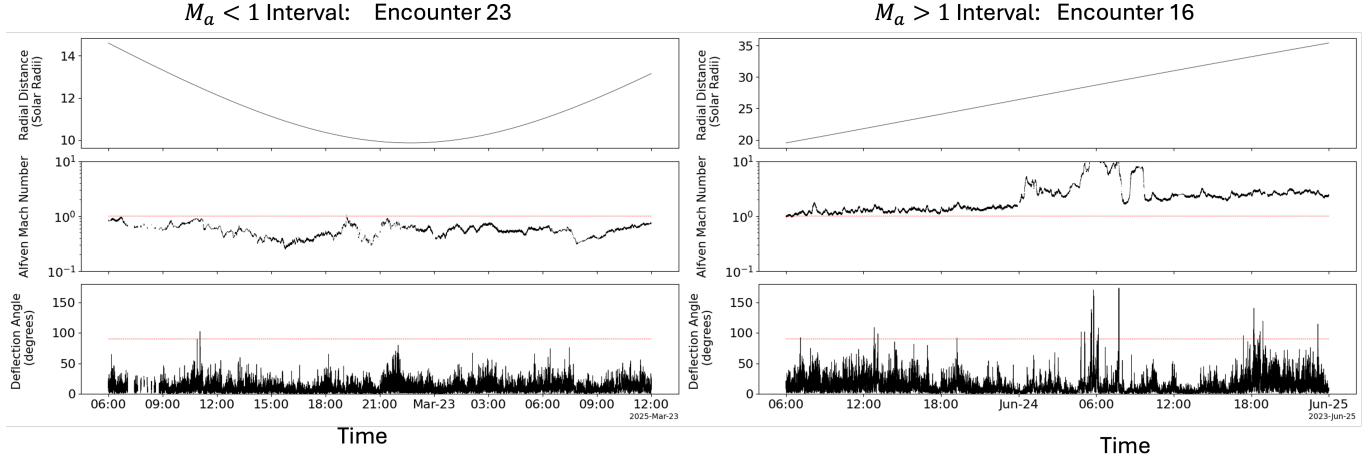


Figure 1. Interval Examples: (a) Sub-Alfvénic Interval from encounter 23 and (b) super-Alfvénic interval from encounter 16. Each example shows, from top to bottom, the heliocentric distance of PSP in units of solar radii, the Alfvénic Mach number with a red dotted line at $M_a = 1$, and the deflection angle with a red dotted line at $\theta_{def} = 90$ degrees.

motion. The radial components of each are expressed below.

$$S_R = \frac{(\vec{E} \times \vec{B})_R}{\mu_0}$$

$$\vec{K}_R = \frac{n_i m_i v_R^2}{2} \vec{v}_R$$

To approximate the electric field in the Poynting flux calculation, we determine the convective electric field using the ion bulk velocity.

$$\vec{E} = \vec{E}_{convective} = -(\vec{v}_i \times \vec{B})$$

In the following sections, we compare a sub- and super-Alfvénic interval, investigate the distribution of magnetic deflection angles with M_a , and examine their velocity and energy flux characteristics.

3. COMPARING A SUB-ALFVÉNIC AND SUPER-ALFVÉNIC INTERVAL

Figure 1 shows examples of a sub-Alfvénic and a super-Alfvénic PSP interval from encounters 23 and 16, respectively. In each set of panels we show the distance of PSP from the sun, the Alfvénic Mach number, and the magnetic deflection angle (θ_{def}). The super-Alfvénic interval has multiple periods with $\theta_{def} > 90$ degrees, while in this particular sub-Alfvénic interval θ_{def} rarely exceeds 90 degrees. While this could imply a relationship between M_a and θ_{def} , it is necessary to investigate the relationship between these two variables across many different encounters spanning a range of M_a values.

4. DISTRIBUTION OF DEFLECTION ANGLES

The distribution of θ_{def} as a function of $\log_{10}(M_a)$ is presented as a 2D histogram in figure 2. The lack of significant $\theta_{def} > 90$ degree data in the sub-Alfvénic regime ($\log_{10}(M_a) < 0$) is consistent with earlier studies Bandyopadhyay et al. (2022); Akhavan-Tafti & Soni (2024); Adhikari et al. (2025) that relied on the earliest sub-Alfvénic encounters by PSP, suggesting that full switchbacks in the sub-Alfvénic regime are exceedingly rare compared to super-Alfvénic intervals. The distribution of the largest θ_{def} with increasing M_a appears fairly continuous, suggesting that magnetic deflection angles tend to become systematically larger with increasing M_a , no matter their originating mechanism. When plotting as a function of distance from the sun, rather than M_a , there is not as obvious a trend, though there is a notable increase in larger deflections beyond ~ 25 solar radii.

5. PROPERTIES OF SUB- AND SUPER-ALFVÉNIC VELOCITY DEFLECTIONS

To further examine the nature of the sub- to super-Alfvénic transition, we explore the properties of velocity fluctuations and energy flux densities associated with the deflections in each regime. Figure 3(a-d) again shows 2D histograms

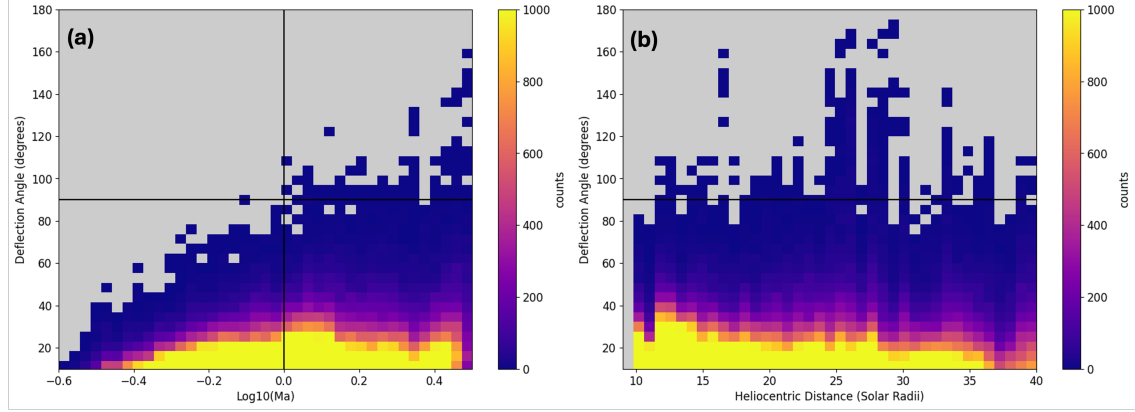


Figure 2. Distribution of Magnetic deflection angles (a) as a function of $\log_{10}(M_a)$ with black lines indicating $M_a = 1$ and $\theta_{def} = 90$ degrees and (b) as a function of Heliocentric distance with a horizontal black line indicating $\theta_{def} = 90$ degrees.

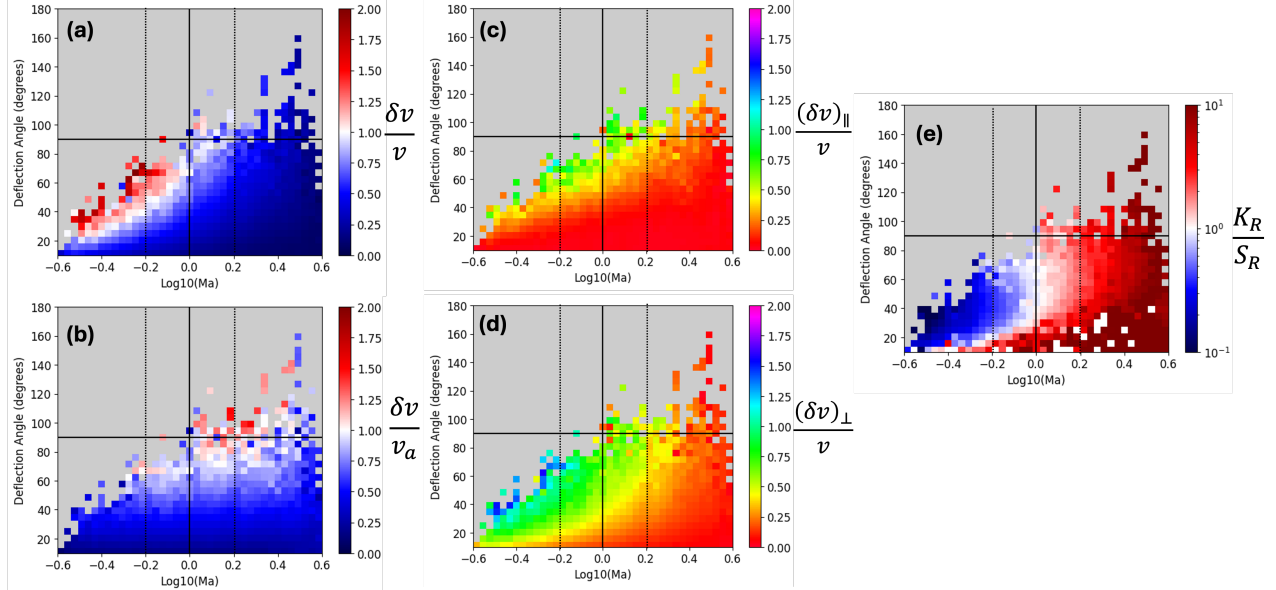


Figure 3. Distribution of velocity deflections with respect to $\log_{10}(M_a)$ and deflection angle normalized to (a) the mean bulk velocity and (b) the mean Alfvén speed. Also included are separate velocity deflection contributions (c) parallel and (d) perpendicular to the mean magnetic field, each normalized to the mean bulk velocity. (e) Ratio of radial ion kinetic energy flux to radial Poynting flux with respect to $\log_{10}(M_a)$ and deflection angle. The solid black lines in all plots indicate the values of $\log_{10}(M_a) = 0$ (or $M_a = 1$) and $\theta_{def} = 90$ degrees. The vertical dotted lines in all plots indicate values of $|\log_{10}(M_a)| = 0.2$ as a visual aid.

of the distribution of deflection angles vs M_a , with $\delta v/v$, $\delta v/v_a$, $(\delta v)_{\parallel}/v$, and $(\delta v)_{\perp}/v$ represented by the color scales. In the sub-Alfvénic regime, the largest θ_{def} values tend to be associated with strong velocity deflections that exceed the bulk velocity magnitude ($\delta v/v > 1$), while the largest deflections in the super-Alfvénic regime tend to have $\delta v/v \lesssim 1$. When normalized to the Alfvén speed, $\delta v/v_a$ rarely exceeds unity in the sub-Alfvénic regime, but $\delta v/v_a \sim 1$ close to the Alfvén surface in the sub-Alfvénic regime, followed by more $\delta v/v_a > 1$ data at large deflection angles in the super-Alfvénic regime. Figure 3(c-d) uses a different color scale to better emphasize how the different components of δv vary in parameter space. The $(\delta v)_{\perp}/v$ contributions tend to dominate and are at their most significant for the largest values of θ_{def} deep in the sub-Alfvénic regime where $\log_{10}(M_a) \lesssim -0.2$. In contrast, the $(\delta v)_{\parallel}/v$ term tends to be at its largest when $|\log_{10}(M_a)| < 0.2$.

The distribution of $\delta v/v$ and its component contributions suggest that within the sub-Alfvénic regime, there is some variability in the nature of the Alfvénic fluctuations as M_a approaches unity. In figure 3e we examine the energy

flux content associated with these fluctuations based on the distribution of K_R/S_R . The larger θ_{def} values in the sub-Alfvénic regime tend to be dominated by S_R while the smaller ones (below ~ 20 degrees) tend to have larger K_R . From $\log_{10}(M_a) \simeq -0.2 - 0$, the the K_R/S_R ratio approaches unity for the largest θ_{def} . In the super-Alfvénic regime, K_R tends to dominate at nearly all deflection angles, especially for $\log_{10}(M_a) > 0.2$.

6. DISCUSSION

We have analyzed the statistics of magnetic deflection angles, velocity deflections, and energy flux densities from a variety of intervals spanning radial distances of $\sim 9.8 - 40$ solar radii with significant data coverage in the range $M_a \sim 0.4 - 2.5$, thus including the $M_a = 1$ threshold that defines the Alfvén surface. Having a variety of radial distances and M_a values is important since the physical location of the Alfvén surface is highly variable (Cranmer et al. 2023; Chhiber et al. 2022), and M_a should not be treated as a direct proxy for radial distance from the solar surface, even if M_a increases with radial distance generally.

The distribution of the largest magnetic deflections (figure 2) systematically increases with M_a and that the largest deflections reach the threshold of $\theta_{def} > 90$ degrees for $\log_{10}(M_a) \geq 0$. These results imply that the upper limit of θ_{def} is somewhat controlled by the local M_a within and near the corona. They also imply that magnetic switchbacks, often defined in part by $\theta_{def} > 90$ degrees (Akhavan-Tafti & Soni 2024), could form through a steepening process that affects Alfvénic structures above and below it. This is consistent with the theory (Toth et al. 2023) that switchback formation is a result of the distortion of spherically polarized Alfvén waves by transverse gradients in the wave speed, which can gradually increase θ_{def} up to and beyond 90 degrees during propagation.

The velocity fluctuations exhibit distinct characteristics across the sub- to super-Alfvénic transition. It is clear from figure 3a that the largest magnetic deflection angles in the sub-Alfvénic regime tend to have velocity fluctuations exceeding the mean bulk velocity ($\delta v/v > 1$), while there are very few cases of $\delta v/v > 1$ in the super-Alfvénic regime. Figure 3b shows that $\delta v/v_a$ approaches unity in the range $\log_{10}(M_a) \sim -0.2 - 0$, but rarely exceeds unity until $\log_{10}(M_a) > 0$. These striking results suggest that near the Alfvén surface, the $\delta v/v_a \sim 1$ criterion may create instabilities that tend to erode large velocity fluctuations ($\delta v/v > 1$) in the super-Alfvénic regime. This is consistent with Ruffolo et al. (2020), who showed that velocity shears near the Alfvén speed allow Kelvin-Helmholtz instabilities to develop when magnetic tension becomes too weak to suppress them, ultimately enhancing turbulence and magnetic deflection angles beyond the Alfvén surface.

Decomposition of the separate components of $\delta v/v$ in figure 3(c-d) show that the influence of $(\delta v)_\perp$ tends to dominate, especially for the largest deflection angles deep in the sub-Alfvénic regime ($\log_{10}(M_a) < -0.2$). For the largest magnetic deflections near the Alfvén surface ($|\log_{10}(M_a)| < 0.2$), the normalized $(\delta v)_\parallel$ fluctuations are at their largest and roughly comparable to the $(\delta v)_\perp$ components. The significant influence of $(\delta v)_\parallel$ in this critical $|\log_{10}(M_a)| < 0.2$ range suggests a departure from purely Alfvénic characteristics to include more magnetosonic behavior consistent with earlier studies of switchback characteristics (Zank et al. 2020).

The radial energy flux ratio K_R/S_R also exhibits dependencies with M_a and θ_{def} . It is clear from figure 3e that in the sub-Alfvénic regime, most of the magnetic deflections have $S_R > K_R$ and K_R/S_R is smaller for larger θ_{def} . The reduced influence of S_R at small θ_{def} makes sense considering that in the $\theta_{def} \sim 0$ limit (assuming background magnetic field dominated by B_R), there are no B_T or B_N components that can contribute to S_R . However, in the range $\log_{10}(M_a) \sim -0.2 - 0$ there is also some reduced influence at the largest values of θ_{def} where the $K_R/S_R \lesssim 1$. From $\log_{10}(M_a) \sim 0 - 0.2$, the contributions from K_R and S_R are roughly comparable for $\theta_{def} \sim 40 - 80$ degrees, but dominated by K_R for $\theta_{def} \lesssim 40$ degrees and $\theta_{def} \gtrsim 80$ degrees. K_R dominates for all deflection angles beyond $\log_{10}(M_a) \sim 0.2$. A simple analysis can help make sense of the result of this transition with M_a . If we take $K \sim nmv^3/2$ and $S \sim EB/\mu_0 \sim vB^2/\mu_0$, then $K/S \sim \mu_0 nmv^2/2B^2 = v^2/2v_a^2 = M_a^2/2$. Setting $K/S = 1$ and solving for M_a we obtain $M_a = \sqrt{2}$ or $\log_{10}(M_a) \simeq 0.15$, which is close to $\log_{10}(M_a) \sim 0.2$ beyond which K_R starts to dominate for all deflections.

These statistical results do not necessarily imply that an individual structure moving across a $M_a = 1$ boundary will suddenly lose most of its velocity shear and electromagnetic energy flux content. However they do imply that Alfvénic deflections tend to undergo a transition in their velocity energy flux characteristics within a conversion layer where $|\log_{10}(M_a)| \lesssim 0.2$. We present a diagram in figure 4 that illustrates the main results of the preceding sections and the observed characteristics of the sub-Alfvénic regime, the super-Alfvénic regime, and the conversion layer (not to scale). Large velocity deflections in the conversion layer become increasingly parallel to the magnetic field and become unstable as δv approaches the Alfvén speed. As this occurs, instabilities like those described in Ruffolo et al. (2020)

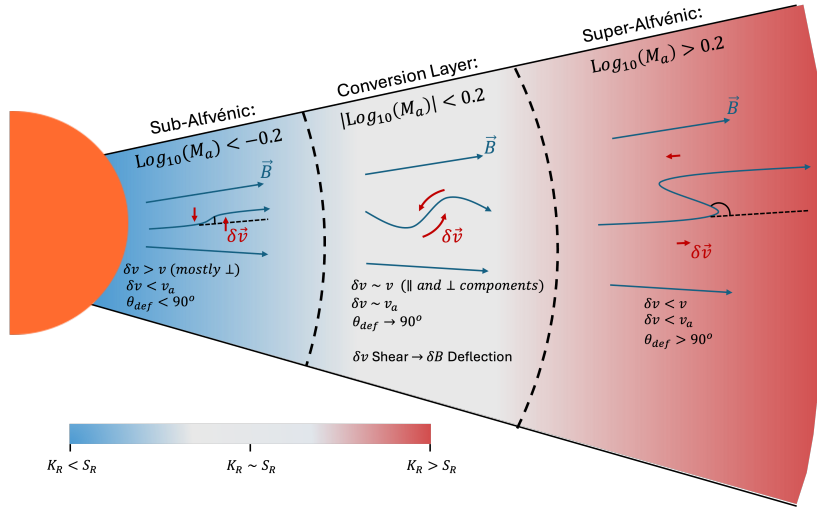


Figure 4. Diagram illustrating the characteristics of the sub-Alfvénic and super-Alfvénic regimes as well as the so-called 'conversion layer' where proximity to the Alfvén surface introduces nonlinear interactions between magnetic and velocity deflections.

can arise which result in the termination of large velocity deflections and can produce large magnetic deflection angles during KH-type roll up processes. Meanwhile, the radial components of the Poynting flux and ion kinetic energy flux densities become comparable in the conversion layer before kinetic energy flux fully dominates in the super-Alfvénic regime.

In conclusion, our study shows that the conversion layer encompassing the Alfvén surface likely plays a role in the formation of magnetic switchbacks (Akhavan-Tafti & Soni 2024) and contributes to the acceleration and heating of solar wind (Akhavan-Tafti et al. 2022; Mostafavi et al. 2025).

Before closing, the authors note a potential challenge to the stated findings of this study; namely the $\theta_{def} > 90$ degree deflection near 11:00 UT in figure 1, which appears to occur in a sub-Alfvénic interval. Upon close inspection of that interval (not shown) we find that there is a small gap in the QTN density data, and therefore the derived M_a , concurrent with this deflection, which explains why this particular sub-Alfvénic deflection exceeding 90 degrees does not show up in the statistical results. Alternate methods for determining M_a to fill in the gap such as smoothing or using SPAN-I density do seem to indicate that the interval could be a genuine outlier where $\theta_{def} < 90$ degrees and $M_a < 1$, but verification and further analysis of this event is beyond the scope of this study. We emphasize that the statistical results of this study do not rule out the possibility of $\theta_{def} < 90$ degree deflections in the sub-Alfvénic regime, but they do suggest such cases are exceedingly rare compared to the super-Alfvénic regime.

7. CONCLUSION

We have examined the statistics of magnetic deflection angles in a variety of sub-Alfvénic and super-Alfvénic solar wind regimes. Our initial finding is that while the distribution of magnetic deflection angles as a function of heliocentric distance may be complicated, the maximum observed magnetic deflection angles are somewhat tied to the local Alfvén Mach number. This demonstrates that large magnetic deflections can result from a steepening process that gradually increases small magnetic deflection angles during propagation eventually resulting in full reversals in super-Alfvénic solar wind. The velocity fluctuations associated with the largest sub-Alfvénic deflection angles tend to exceed the background flow magnitude, but such large velocity deflections tend not to survive into the super-Alfvénic regime, even for the largest magnetic deflection angles. Further decomposition of the parallel and perpendicular components of the velocity deflections in the sub-Alfvénic regime suggests that while they are mainly dominated by perturbations perpendicular to the local magnetic field, parallel perturbations play an increasing role as the sub-Alfvénic mach number approaches unity, suggesting a mixture of Alfvénic and magnetosonic characteristics. The distribution of the energy flux ratio suggests that below the Alfvén surface, the Poynting flux density tends to dominate for all but the smallest deflection angles, but the kinetic energy flux dominates for $\log_{10}(M_a) > 0.2$. These results demonstrate that while full switchback production may not be entirely localized precisely at a $M_a = 1$ boundary, there exists what we

refer to as the conversion layer ($|\log_{10}(M_a)| \lesssim 0.2$) which contributes to switchback formation and field-particle energy conversion.

ACKNOWLEDGMENTS

This work was primarily supported by NASA contract number NNN06AA01C. This work would not be possible without the entirety of the PSP team, including those that keep the instrumentation operational and those involved in data management.

DATA AVAILABILITY

The PSP data used in this study is publicly available from the Coordinated Data Analysis Web (<https://cdaweb.gsfc.nasa.gov/public/>).

REFERENCES

Adhikari, S., Bandyopadhyay, R., Goodwill, J., et al. 2025, arXiv preprint arXiv:2510.07472

Akhavan-Tafti, M., Kasper, J., Huang, J., & Bale, S. 2021, *Astronomy & Astrophysics*, 650, A4

Akhavan-Tafti, M., Kasper, J., Huang, J., & Thomas, L. 2022, *The Astrophysical Journal Letters*, 937, L39

Akhavan-Tafti, M., & Soni, S. 2024, *The Astrophysical Journal Letters*, 970, L26

Bale, S., Goetz, K., Harvey, P., et al. 2016, *Space science reviews*, 204, 49

Bale, S., Badman, S., Bonnell, J., et al. 2019, *Nature*, 576, 237

Bandyopadhyay, R., Matthaeus, W., McComas, D., et al. 2022, *The Astrophysical journal letters*, 926, L1

Chhiber, R., Matthaeus, W. H., Usmanov, A. V., Bandyopadhyay, R., & Goldstein, M. L. 2022, *Monthly Notices of the Royal Astronomical Society*, 513, 159

Chhiber, R., Pecora, F., Usmanov, A. V., et al. 2024, *Monthly Notices of the Royal Astronomical Society: Letters*, 533, L70

Cranmer, S. R., Chhiber, R., Gilly, C. R., et al. 2023, *Solar Physics*, 298, 126

de Wit, T. D., Krasnoselskikh, V. V., Bale, S. D., et al. 2020, *The Astrophysical Journal Supplement Series*, 246, 39

Goodwill, J., Adhikari, S., Payne, D., et al. 2025, *Parker Solar Probe Analysis across the Alfvénic Transition: Velocity Shear, Magnetic Deflection and Switchback Formation*

Kasper, J. C., Abiad, R., Austin, G., et al. 2016, *Space Science Reviews*, 204, 131

Kasper, J. C., Bale, S. D., Belcher, J. W., et al. 2019, *Nature*, 576, 228

Livi, R., Larson, D. E., Kasper, J. C., et al. 2022, *The Astrophysical Journal*, 938, 138

Mostafavi, P., Jagarlamudi, V., Raouafi, N., et al. 2025, *The Astrophysical Journal Letters*, 991, L35

Pulupa, M., Bale, S., Bonnell, J., et al. 2017, *Journal of Geophysical Research: Space Physics*, 122, 2836

Ruffolo, D., Matthaeus, W. H., Chhiber, R., et al. 2020, *The Astrophysical Journal*, 902, 94

Toth, G., Velli, M., & van der Holst, B. 2023, *The Astrophysical Journal*, 957, 95

Zank, G., Nakanotani, M., Zhao, L.-L., Adhikari, L., & Kasper, J. 2020, *The Astrophysical Journal*, 903, 1